IEEE Access
Multidisciplinary | Rapid Review | Open Access Journal

Received June 21, 2019, accepted July 30, 2019, date of publication August 2, 2019, date of current version August 19, 2019.

Digital Object Identifier 10.1109/ACCESS.2019.2932794

Global Identification of FitzHugh-Nagumo Equation via Deterministic Learning and Interpolation

XUNDE DONG[1], WENJIE SI[2], AND CONG WANG[1]
[1]School of Automation Science and Engineering, South China University of Technology, Guangzhou 510641, China
[2]School of Electrical and Control Engineering, Henan University of Urban Construction, Pingdingshan 467036, China

Corresponding author: Cong Wang (wangcong@scut.edu.cn)

This work was supported in part by the Natural Science Foundation of Guangdong Province, China, under Grant 2018A030310367 and Grant 2017A030310493, in part by the Fundamental Research Funds for the Central Universities under Grant 2018A030310367, in part by the National Natural Science Foundation of China under Grant 61527811, and in part by the Science and Technology Program of Guangzhou, China, under Grant 201704020078.

ABSTRACT Spiral wave is closely related to the occurrence of malignant ventricular arrhythmia. It is important and necessary to study the spiral wave dynamics to better analyze and control spiral waves. In this paper, the dynamics of FitzHugh-Nagumo(FHN) model is identified by using a novel method based on deterministic learning and interpolation method. The FHN model, which has been studied extensively in physical and mathematical science, is often used to study spiral waves. It is a distributed parameter (DPS) described by two coupled partial differential equations (PDEs). To identify the underlying system dynamics of the FHN model globally, we first transform the FHN model into a set of ordinary differential equations (ODEs) by applying the method of lines. Then, we identify the dynamics of the approximation system by employing deterministic learning. That is, the FHN dynamics on a set of spatial grid nodes is accurately identified. To achieve the global identification of the FHN model, the underlying system dynamics of the FHN model on any other spatial point is approximated via an algorithm based on the interpolation method. The effectiveness and feasibility of the proposed method are demonstrated theoretically and numerically.

INDEX TERMS Dynamics, system identification, radial basis function networks, interpolation.

I. INTRODUCTION

Spiral waves are one of the most typical two-dimensional spatiotemporal patterns in excitable or oscillatory reaction-diffusion systems, which can be observed in a variety of chemical and biological systems. Studies have shown that the ventricular tachycardia and fibrillation are often regarded as the results of the breakup of spiral waves in cardiac muscle [1]–[3]. It is important and necessary to study the dynamics of spiral waves, which may propose ideas in prevention and treatment of ventricular tachycardia and fibrillation. The FitzHugh-Nagumo(FHN) model [4], [5], a simplified modification of the famous Hodgkin-Huxley model (the first mathematical model of myocardial cell) [6], has been used as a classic model for decades in the study of spiral waves in excitable media [7], [8]. In addition, it is also useful for the study of biology, genetics, and heat and mass transfer systems [9]. The chaos and synchronization of the FHN model have potential applications value in several fields, including medicine, laser technology, chemistry, and secure communication [10]. Therefore, it is of great significance to study the dynamics of FHN model in practical application.

It is noted that the FHN model is described by two coupled PDEs, the identification of the FHN model is virtually a problem of distributed parameter system (DPS) identification. In general, the researches on DPS identification can be classified as two categories [11]: (a) the system structure of DPS is known while system parameters are unknown; (b) both system structure and parameters of DPS are unknown, which is very common in the real world. For the first case, it just needs to identify the system parameters of DPS. For the second case, both the system structure and parameters of DPS have to be identified. Parameter identification, which means for the determination of unknown parameters from observed data in the sense that the predicted output is close to the observed data on some criteria, is the fundamental issues in

The associate editor coordinating the review of this manuscript and approving it for publication was Bora Onat.

This work is licensed under a Creative Commons Attribution 4.0 License. For more information, see http://creativecommons.org/licenses/by/4.0/

DPS identification [12], [13] (e.g., parameter estimation in mechanical systems [14]–[16], spatially extended systems [17], flow reactors [18]). There is also much research on parameter identification of the FHN model, which is important for analyzing the dynamical behavior of the FHN model [10], [19]–[22]. When the PDE description of the DPS is known, it can be easily transformed into an infinite-dimensional system of ordinary differential equation or difference equation (DE). Then the model reduction will be critical to derive a low-order model for practical application.

Persistent excitation (PE) condition is an essential condition to ensure parameter convergence in both lumped parameter system identification and DPS identification. Nevertheless, the PE condition is normally hard to be satisfied and cannot be verified in advance for the identification of general nonlinear dynamical systems. Recently, a novel method, named deterministic learning, was proposed to identify the dynamics of general nonlinear dynamical systems [23]. It has proved that the partial PE condition can be satisfied along the recurrent orbits by applying the localized RBF networks, where the recurrent orbit represents a large set of periodic, quasiperiodic, almost-periodic, and even chaotic orbits generated from nonlinear dynamical systems (strict definition of the recurrent orbit can be seen in [24]). With the partial PE condition, the accurate identification of system dynamics can be achieved along the recurrent orbits [25]–[27].

In our previous work [28], system dynamics of the FHN model has been identified at a set of finite spatial points. In our other work [29], a novel system identification method based on deterministic learning and interpolation method had been proposed to identify a one-dimensional DPS. In this work, we will study global identification of FHN model, which means to achieve accurate identification of FHN model on any spatial point, based on the methods proposed in [28] and [29]. System dynamics of the FHN model can be regarded as an infinite-dimensional continuous differentiable function vector since it is described by two coupled PDEs. The infinite-dimensional property makes it hard to identify system dynamics of the FHN model by applying neural networks directly. To overcome the problem, the model reduction is essential for FHN model. Therefore, we first divide the space domain of FHN model into a set of subdomains by a set of spatial grid nodes and approximate the spatial derivatives by employing the method of lines (a special case of the finite difference method). That is, the FHN model is approximated by a set of ODEs. Second, we identify the dynamics of ODEs by employing deterministic leaning theory. The dynamics underlying recurrent orbits of spiral waves corresponding to the grid nodes can be accurately identified and represented as a constant manner. Third, we approximate the FHN model dynamics at any other spatial point by applying interpolation method based on the identification results corresponding to the grid nodes. That is, the global identification of FHN model is achieved, accurate identification of the FHN model at any spatial point can be achieved.

Compared with other studies on identification of FHN model, the features of the proposed method, including: (a) The underlying system dynamics of FHN model is identified globally only based on the system state at a set of spatial grid point via deterministic learning and interpolation; (b) It has important significance in the possible application of the method (e.g., the study of spiral wave in cardiac tissue) as two-dimensional DPS is more common than one-dimensional DPS in practice, it may provide new ways for the DPS identification in industry; (c) The obtained knowledge contains complete information on both states and system dynamics of FHN model. Information of system states, structure and parameters of the FHN model is also included; (d) The obtained knowledge is stored by constant RBF networks, which makes it easy to be employed to recognize the similar dynamical behaviors.

The remaining part of this paper is organized as follows. Deterministic learning theory and polynomial interpolation methods will be introduced briefly in Section 2. The proposed method is demonstrated in Section 3. Numerical results are discussed in Section 4. Finally, Section 5 concludes the paper.

II. PRELIMINARY

A. DETERMINISTIC LEARNING

Deterministic learning theory is a machine learning method recently proposed for the identification and recognition of temporal patterns [25]. It was principally developed based on the knowledge of RBF networks, adaptive control and system identification. For a temporal pattern, which is defined as a periodic or recurrent orbit generated by nonlinear dynamical systems, the fundamental knowledge of the temporal pattern can be accurate identified and stored as a time-invariant manner [26], [27].

Consider the following dynamical system:

$$\dot{u} = G(u; p), \quad u(t_0) = u_0 \tag{1}$$

where $u = [u_1, \ldots, u_n]^T \in R^n$ is the system state, $G(u; p) = [g_1(u; p), \ldots, g_n(u; p)]^T$ is a continuous but unknown nonlinear function vector, and p is a constant parameter vector.

In order to accurately model the unknown system dynamics $G(u; p)$ underlying a dynamical pattern φ_ζ (a recurrent orbit), the following estimator system is applied:

$$\dot{\hat{u}}_i = -d_i(\hat{u}_i - u_i) + \hat{W}_i^T S_i(u), \tag{2}$$

where u_i and $\hat{u}_i$ are states of (1) and (2) respectively, $d_i > 0$ is a parameter to be designed, RBF networks $\hat{W}_i^T S_i(u)$ is used to approximate $g_i(u; p)$, $\hat{W}_i = [w_{i1}, \ldots, w_{iN}]^T \in R^N$ and $S_i(u) = [s_{i1}(\| u - \xi_1 \|), \ldots, s_{iN}(\| u - \xi_N \|)]^T$, ξ_j are distinct points in state space, $s_{ij}(\cdot)$ is Gaussian function.

Subtract Eq.(1) from Eq.(2), the following equation can be obtained:

$$\begin{aligned} \dot{\tilde{u}}_i &= -d_i\tilde{u}_i + \hat{W}_i^T S_i(u) - g_i(u; p) \\ &= -d_i\tilde{u}_i + \tilde{W}_i^T S_i(u) - e_i, \end{aligned} \tag{3}$$

where $\tilde{u}_i = \hat{u}_i - u_i$ is state estimation error, $\tilde{W}_i = \hat{W}_i - W_i^*$, W_i^* is the ideal constant weight vector, $e_i = g_i(u; p) - W_i^{*T} S_i(u)$ is the ideal approximation error. To update $\hat{W}_i$, the following Lyapunov-based learning law was employed:

$$\dot{\hat{W}}_i = -\gamma_i S_i(u)\tilde{u}_i - \sigma_i \gamma_i \hat{W}_i, \tag{4}$$

where $\sigma_i > 0$ is a small constant parameter, $\gamma_i = \gamma_i^T > 0$.

It has proved that for almost any temporal pattern (recurrent orbit) φ_ζ, the accurate identification of unknown dynamics $g_i(u; p)$ along the orbit φ_ζ can be achieved [25]–[27] and represented as follow:

$$\begin{aligned} g_i(\varphi_\zeta; p) &= \hat{W}_i^T S_i(\varphi_\zeta) + e_{\zeta i} \\ &= \bar{W}_i^T S_i(\varphi_\zeta) + e_{\zeta i1}, \end{aligned} \tag{5}$$

where $\bar{W}_i = mean_{t\in[t_s,t_f]}\hat{W}_i(t)$, *mean* is the arithmetic mean, $[t_s, t_f]$ is a span of time after the transient process, $e_{\zeta i1} = O(e_{\zeta i}) = O(e_i)$ is the actual modeling error. It indicates the dynamics underlying almost any temporal pattern can be accurately modeled by empolying deterministic learning.

B. POLYNOMIAL INTERPOLATION

Interpolation is an essential mathematical tool that plays an important role in scientific and technical calculation. Specifically, it is a vital part of many mathematical algorithms and methods. Polynomial interpolation is one of the most popular interpolation methods since polynomials are easy to construct and evaluate, easy to multiply and sum, easy to integrate and differentiate, and have a variety of properties [30]. In many cases, it is seen that polynomial oscillates varyingly but the function varies smoothly [30]. To overcome this problem, spline function, which is a function of polynomial bits joined together, is considered. The cubic spline interpolation is the most frequently used spline interpolation since it has sufficient flexibility, and the interpolant is continuously differentiable in the interval and has continuous second derivative [31]. The bicubic spline is defined as the product of two one-dimensional cubic splines. It is a usual method that is well-known and extensively applied since it gives more smoother surface than nearest-neighbor or bilinear interpolation method [32]. A two variable cubic spline interpolation of a function $f(x, y)$ is the fitting of a unique series of cubic splines for a given set of data points (x_i, y_j, f_{ij}). The points (x, y) at which $f(x, y)$ are known based on the grid points in $x - y$ plane.

Remark 1: Though there are many interpolation methods and algorithms in literature, none of these methods is better than all other methods for all issues. There are no criteria to evaluate which interpolation algorithm is superior to all other algorithms [33]. The selection of the interpolation algorithm has to consider multiple factors comprehensively, such as computing consuming, data type and desired accuracy [34]. Since the purpose of the paper is to propose a new method for the global identification of FHN model, the selection of interpolation method is not discussed intensively in this paper.

III. METHODS

Consider the following FHN model:

$$\begin{cases} \dfrac{\partial u}{\partial t} = \dfrac{1}{\epsilon}u(u-1)[u - \dfrac{v+b}{a}] + \nabla^2 u \\ \dfrac{\partial v}{\partial t} = u^m - v \end{cases} \tag{6}$$

where $u = u(x, y, t)$ and $v = v(x, y, t)$ are system states, ϵ represents the time ratio between u and v, a, b, m are system parameters, $\nabla^2 = \frac{\partial}{\partial x^2} + \frac{\partial}{\partial y^2}$ is Laplace operator.

Remark 2: There has been a lot of research on the existence of spiral wave solutions of FHN model, their characteristics and behaviors that vary with parameters [35]. It has been shown that for different parameters the spiral waves generated by the FHN model can behave different dynamical behaviors, periodic rotation or quasiperiodic rotation. The spiral wave orbit at any spatial point is recurrent.

Consider $(x, y) \in \Omega = [-L, L] \times [-L, L]$, and evenly subdivide the rectangle Ω into the following $(N-1)\times(N-1)$ subrectangles:

$$\Omega_{ij} = (x, y) : x_i \le x \le x_{i+1}, \quad y_j \le y \le y_{j+1}$$

with the following $(N-1) \times (N-1)$ internal grid nodes:

$$\begin{aligned} -L = x_1 < x_2 < \cdots \le x_N = L, \quad x_i = -L + (i-1)\cdot h_x \\ -L = y_1 < y_2 < \cdots \le y_N = L, \quad y_j = -L + (j-1)\cdot h_y \end{aligned}$$

where $h_x = h_y = h = 2L/(N-1)$. For simplicity, denote $u_{i,j} = u(x_i, y_j, t)$, then we can approximate the Laplacian $\nabla^2 u$ at (x_i, y_j) by using the method of lines as follow:

$$\nabla^2 u_{i,j} = \frac{u_{i,j-1} + u_{i,j+1} + u_{i+1,j} + u_{i-1,j} - 4u_{i,j}}{h^2} + O(h^2) \tag{7}$$

Thus, we can approximate the system (6) at the grid node (x_i, y_j) as the following system:

$$\begin{cases} \dot{u}_{i,j} = F_1(u_{i,j}, v_{i,j}; p_1) \\ \dot{v}_{i,j} = F_2(u_{i,j}, v_{i,j}; p_2) \end{cases} \tag{8}$$

where $u_{i,j} = u(x_i, y_j, t)$, $v_{i,j} = v(x_i, y_j, t)$, $F_1(u_{i,j}, v_{i,j}; p_1) = f(u_{i,j}, v_{i,j}) + \frac{1}{h^2}(u_{i-1,j} + u_{i+1,j} + u_{i,j+1} + u_{i,j-1} - 4u_{i,j})$, $F_2(u_{i,j}, v_{i,j}; p_2) = g(u_{i,j}, v_{i,j})$, $p_1 = [a, b, \epsilon]$ and $p_2 = m$ represents the parameters of (6). That is, we transform the infinite-dimensional FHN model described by PDEs into a finite-dimensional dynamical system described by a set of ODEs.

A. LOCAL IDENTIFICATION

In this subsection, the underlying system dynamics of FHN model at the spatial grid nodes will be identified first, which is called "local identification". We employ the following two dynamical models to identify the system dynamics $F_1(u_{i,j}, v_{i,j}; p_1)$ and $F_2(u_{i,j}, v_{i,j}; p_2)$ of the approximation

system (8):

$$\begin{cases} \dot{\hat{u}}_{i,j} = -a_1(\hat{u}_{i,j} - u_{i,j}) + \hat{W}_1^T S_1(U_{i,j}) \\ \dot{\hat{v}}_{i,j} = -a_2(\hat{v}_{i,j} - v_{i,j}) + \hat{W}_2^T S_2(V_{i,j}) \end{cases} \tag{9}$$

where $U_{i,j} = [u_{i-1,j}, u_{i+1,j}, u_{i,j-1}, u_{i,j+1}, u_{i,j}, v_{i,j}]$, $V_{i,j} = [u_{i,j}, v_{i,j}]$, $\hat{u}_{i,j}$ and $\hat{v}_{i,j}$ are the estimation of $u_{i,j}$ and $v_{i,j}$ in system (8) respectively, $a_1 > 0$ and $a_2 > 0$ are design constants, RBF networks $\hat{W}_1^T S_1(U_{i,j})$ and $\hat{W}_2^T S_2(V_{i,j})$ are used to approximate $F_1(u_{i,j}, v_{i,j}; p_1)$ and $F_2(u_{i,j}, v_{i,j}; p_2)$.

Remark 3: Though there is no strict definition of the system dynamics of DPS, it can be regarded as the infinite-dimensional continuously differentiable vector function of the infinite-dimensional dynamical system (i.e., the DPS that often described by PDEs or integral equation) [36]. The dynamics of the FHN model (6) are $\frac{1}{\epsilon}u(u-1)[u-\frac{v+b}{a}]+\nabla^2 u$ and $u^m - v$.

From equations (8) and (9), the derivative of the state estimation errors $\tilde{u}_{i,j} = \hat{u}_{i,j} - u_{i,j}$ and $\tilde{v}_{i,j} = \hat{v}_{i,j} - v_{i,j}$ satisfy:

$$\begin{cases} \dot{\tilde{u}}_{i,j} = -a_1\tilde{u}_{i,j} + \hat{W}_1^T S_1(U_{i,j}) - F_1(u_{i,j}, v_{i,j}; p_1) \\ \quad = -a_1\tilde{u}_{i,j} + \tilde{W}_1^T S_1(U_{i,j}) - \epsilon_{1ij} \\ \dot{\tilde{v}}_{i,j} = -a_2\tilde{v}_{i,j} + \hat{W}_2^T S_2(V_{i,j}) - F_2(u_{i,j}, v_{i,j}; p_2) \\ \quad = -a_2\tilde{v}_{i,j} + \tilde{W}_2^T S_2(V_{i,j}) - \epsilon_{2ij} \end{cases} \tag{10}$$

where $\hat{W}_l$ is the estimate of $W_l^*(l = 1, 2)$, $\tilde{W}_l = \hat{W}_l - W_l^*$, and $\epsilon_{1ij} = F_1(u_{i,j}, v_{i,j}; p_1) - W_1^{*T} S_1(U_{i,j})$, $\epsilon_{2ij} = F_2(u_{i,j}, v_{i,j}; p_2) - W_2^{*T} S_2(V_{i,j})$ are the ideal approximation errors. The following law is employed to update $\hat{W}_1$ and $\hat{W}_2$:

$$\begin{cases} \dot{\hat{W}}_1 = \dot{\tilde{W}}_1 = -\Gamma_1 S_1(U_{i,j})\tilde{u}_{i,j} - \sigma_1\Gamma_1\hat{W}_1 \\ \dot{\hat{W}}_2 = \dot{\tilde{W}}_2 = -\Gamma_2 S_2(V_{i,j})\tilde{v}_{i,j} - \sigma_2\Gamma_2\hat{W}_2 \end{cases} \tag{11}$$

where $\Gamma_1 = \Gamma_1^T > 0, \Gamma_2 = \Gamma_2^T > 0$ and $\sigma_1 > 0, \sigma_2 > 0$ are small values.

The following theorem manifests that $F_1(u_{i,j}, v_{i,j}; p_1)$ and $F_2(u_{i,j}, v_{i,j}; p_2)$ can be accurately identified along the recurrent orbit at spatial grid nodes (x_i, y_j).

Theorem 4: [28] Consider the adaptive system composed of (8), (9) and (11), we have: (i) $\tilde{u}_{i,j}$ and $\tilde{v}_{i,j}$ converge to a small neighborhood of zero, and $\hat{W}_1$ and $\hat{W}_2$ converge to small neighborhoods of $\hat{W}_l^*$ and $\hat{W}_2^*$; (ii) accurate approximation of $F_1(u_{i,j}, v_{i,j}; p_1)$ and $F_2(u_{i,j}, v_{i,j}; p_2)$ can be attained along the recurrent orbit at spatial grid node (x_i, y_j).

$$\begin{cases} F_1(u_{i,j}, v_{i,j}; p_1) = \bar{W}_1^T S_1 + \epsilon_{1_e} \\ F_2(u_{i,j}, v_{i,j}; p_2) = \bar{W}_2^T S_2 + \epsilon_{2_e} \end{cases} \tag{12}$$

where ϵ_{1_e} and ϵ_{2_e} are the practical approximation error along the trajectory corresponding to spatial point (x_i, y_j).

Remark 5: FHN model is often used for studying spiral waves, which is a representative of the two-dimensional spatiotemporal patterns with recurrent orbit. Under different parameter conditions, different spiral waves can be generated by FHN model, such as rotating spiral wave (periodic orbit), modulated rotating spiral wave (quasiperiodic orbit), meandering spiral wave (chaotic orbit). That is, for any given spatial point (x, y), $u(x, y, t)$ and $v(x, y, t)$ are recurrent in time. Thus, the partial PE condition can be satisfied along the recurrent orbits at spatial grid nodes (x_i, y_j) by applying the localized RBF networks, which makes the achievement of local identification of the FHN model.

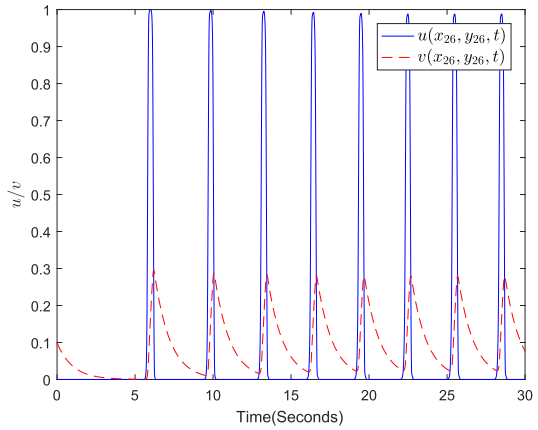

FIGURE 1. The trajectories of $u(x_{26}, y_{26}, t)$ and $v(x_{26}, y_{26}, t)$.

B. GLOBAL IDENTIFICATION

Based on the local identification of FHN model, in the subsection we will achieve the global identification of FHN model by employed interpolation method. To differentiate the notation from the spatial grid nodes involving in the above subsection, replace the spatial variable $U_{i,j}$ and $V_{i,j}$ in (11) with $U(x, y)$ and $V(x, y)$, where (x, y) is any given spatial point barring the grid nodes (x_i, y_j), thus $U(x, y, t)$ and $V(x, y, t)$ can be treated as one-variable function of t. Then (11) can be rewritten as follows:

$$\begin{cases} \dot{\hat{W}}_1(x, y, t) = -\Gamma_1 S_1(U(x, y, t))\tilde{u}(x, y, t) - \sigma_1\Gamma_1\hat{W}_1 \\ \dot{\hat{W}}_2(x, y, t) = -\Gamma_2 S_2(V(x, y, t))\tilde{v}(x, y, t) - \sigma_2\Gamma_2\hat{W}_2 \end{cases} \tag{13}$$

The following equations can be obtained by solving the partial differential equations (13):

$$\begin{cases} \hat{W}_1(x, y, t) = e^{-\sigma_1\Gamma_1 t}(C_1 \\ \quad - \int \Gamma_1 S_1(U(x, y, t))\tilde{u}(x, y, t)e^{-\sigma\Gamma t}dt) \\ \hat{W}_2(x, y, t) = e^{-\sigma_2\Gamma_2 t}(C_2 \\ \quad - \int \Gamma_2 S_2(V(x, y, t))\tilde{v}(x, y, t)e^{-\sigma\Gamma t}dt) \end{cases} \tag{14}$$

where C_1, C_2 are constants, $\tilde{u}(x, y, t) = \hat{u}(x, y, t) - u(x, y, t)$, $\tilde{v}(x, y, t) = \hat{v}(x, y, t) - v(x, y, t)$.

To achieve the accurate identification of FHN model globally, the following Lemma and two theorems are first given.

Lemma 6: [37] Let $f(x, y) \in C^{(4,4)}[\Omega]$, where $\Omega = [x_0, x_n] \times [y_0, y_{n'}]$. Then

$$\|(f - s_f)\|_\infty \le \frac{5}{384}\|f^{(4,0)}\|_\infty h_x^4 + \frac{81}{64}\|f^{(2,2)}\|_\infty h_x^2 h_y^2 + \frac{5}{384}\|f^{(0,4)}\|_\infty h_y^4, \quad 0 \le k, l \le 2 \tag{15}$$

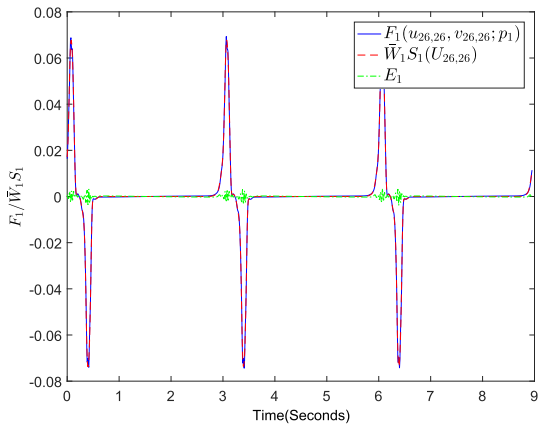

(a) The approximation of $F_1(u, v; p_1)$.

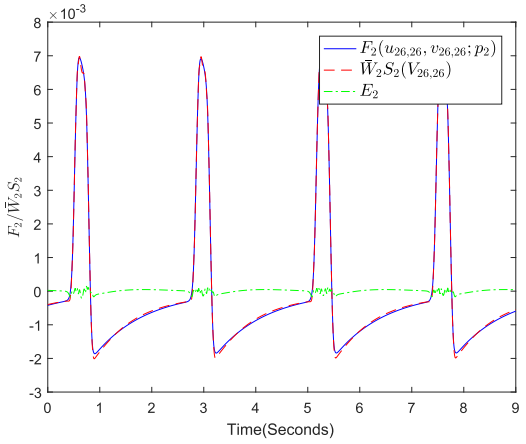

(b) The approximation of $F_2(u, v; p_2)$.

FIGURE 2. The identification results of $F_1(u, v; p_1)$ and $F_2(u, v; p_2)$ at the spatial point (x_{26}, y_{26}) corresponding to $h = 0.6$.

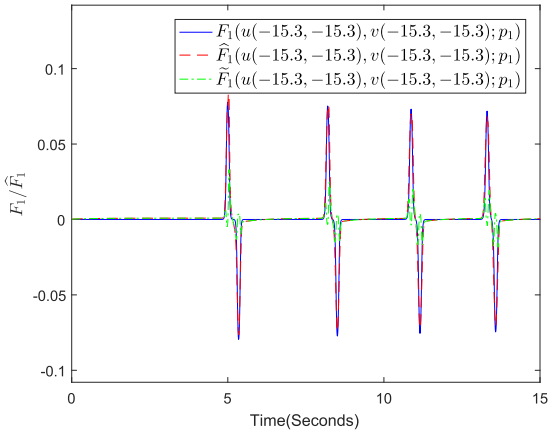

(a) The approximation of $F_1(u, v; p_1)$

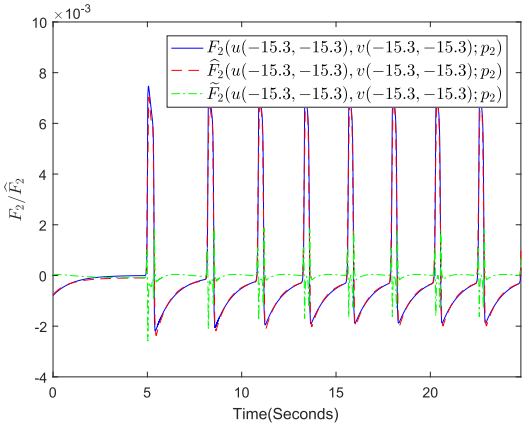

(b) The approximation of $F_2(u, v; p_2)$

FIGURE 3. The approximation of $F_1(u, v; p_1)$ and $F_2(u, v; p_2)$ with periodic $u(x, y, t)$ and $v(x, y, t)$ at spatial point $(-15.3, -15.3)$.

where s_f be the bicubic spline interpolant of $f \in C^{(4,4)}[\Omega]$, $h_x = \max_{0\le i\le n-1}(x_{i+1} - x_i)$, $h_y = \max_{0\le j\le n'-1}(y_{j+1} - y_j)$.

Theorem 7: $\hat{W}_1(x, y, t)$, $\hat{W}_2(x, y, t)$, $S_1(U(x, y, t))$ and $S_2(V(x, y, t)) \in C^4[\Omega] \times [0, \infty)$, and $\hat{W}_1^{(k,l)}(x, y, t)$, $\hat{W}_2^{(k,l)}(x, y, t)$, $S_1^{(k,l)}(U(x, y, t))$ and $S_2^{(k,l)}(V(x, y, t))$ are bounded in Ω, where $0 \le k, l \le 4$ are integers, $\Omega = [-L, L] \times [-L, L]$.

Proof: Please see the appendix A. ■

Based on the Theorem 4, Theorem 7 and Lemma 6, the following theorem gives the identification method of FHN model system dynamics at any spatial point (x, y) based on the identification results corresponding the grid nodes.

Theorem 8: The dynamics of (6) $F_I(u, v, p_I)(I = 1, 2)$ can be approximated as the following equation:

$$\begin{cases} F_1(u, v; p_1) = W_{1C}(x, y, T)S_{1C}(x, y, T) + \epsilon_{N_1}(x) \\ F_2(u, v; p_2) = W_{2C}(x, y, T)S_{2C}(x, y, T) + \epsilon_{N_2}(x) \end{cases} \tag{16}$$

where $W_{IC}(x, y, T)$ is bicubic spline interpolation of $\hat{W}_I(x, y, T)$, $S_{1C}(x, y, T)$ and $S_{2C}(x, y, T)$ are bicubic spline interpolation of $S_1(U(x, y, T))$ and $S_2(V(x, y, T))$,

$$\begin{cases} \epsilon_{N_1}(x) = W_{1C}(x, y, T)R_{1S}(x, y, T) \\ +R_{1W}(x, y, T)S_1(U(x, y, T)) + O(\epsilon) \\ \epsilon_{N_2}(x) = W_{2C}(x, y, T)R_{2S}(x, y, T) \\ +R_{2W}(x, y, T)S_2(V(x, y, T)) + O(\epsilon) \end{cases}$$

are approximation errors, $R_{IW}(x, y, T) = W_I(x, y, T) - W_{IC}(x, y, T)$, $R_{1S}(x, y, T) = S_1(U(x, y, T)) - S_{1C}(x, y, T)$, $R_{2S}(x, y, T) = S_2(V(x, y, T)) - S_{2C}(x, y, T)$, and

$$\begin{aligned} \|\epsilon_{N_I}(x)\|_\infty \le & \frac{5h_x^4}{384}(\mathbf{W}_I^{4,0} + \mathbf{S}_I^{4,0}\|W_{IC}(x, y, T)\|_\infty) \\ & + \frac{81h_x^2h_y^2}{64}(\mathbf{W}_I^{2,2} + \mathbf{S}_I^{2,2}\|W_{IC}(x, y, T)\|_\infty \\ & + \frac{5h_y^4}{384}(\mathbf{W}_I^{0,4} + \mathbf{S}_I^{0,4}\|W_{IC}(x, y, T)\|_\infty) + O(\epsilon_I), \end{aligned} \tag{17}$$

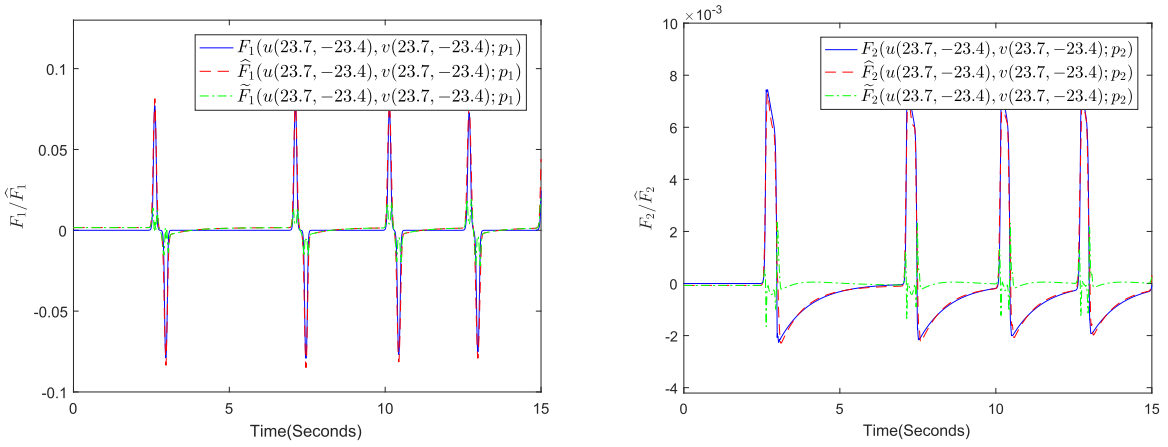

(a) The approximation of $F_1(u, v; p_1)$ (b) The approximation of $F_2(u, v; p_1)$

FIGURE 4. The approximation of $F_1(u, v; p_1)$ and $F_2(u, v; p_2)$ with periodic $u(x, y, t)$ and $v(x, y, t)$ at spatial point (23.7, −20.7).

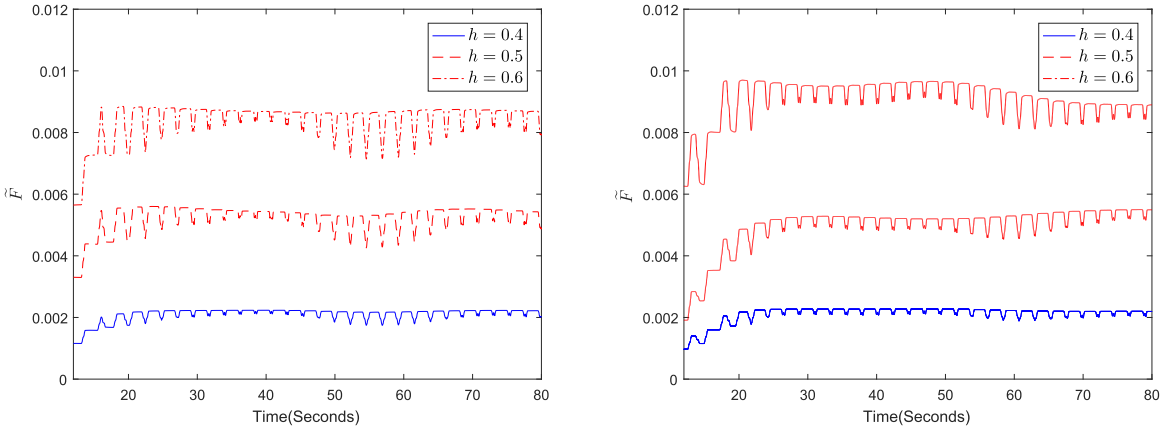

(a) (b)

FIGURE 5. The approximation performance comparison of different h. a: $\|\widetilde{F}(u(-15.3,-15.3), v(-15.3,-15.3))\|_{L_1}$ corresponding to different h; b: $\|\widetilde{F}(u(23.7,-20.7), v(23.7,-20.7))\|_{L_1}$ corresponding to different h.

where ϵ_I is the ideal approximation error of $F_I(u, v, p_I)$ by employing RBF network, which can be made arbitrarily small.

Proof: Please see the appendix B. ■

Remark 9: It can be seen from (17) that the approximation errors strongly depend on the mesh spacing h. The approximation errors $\epsilon_{N1}(x)$, $\epsilon_{N2}(x)$ are in proportion to h^4 under given parameters σ, Γ and C, the smaller h the smaller $\epsilon_{N1}(x)$, $\epsilon_{N2}(x)$. In practice, the determination of h needs to take into account various factors comprehensively, such as accuracy requirement, system formation, and even computing resources.

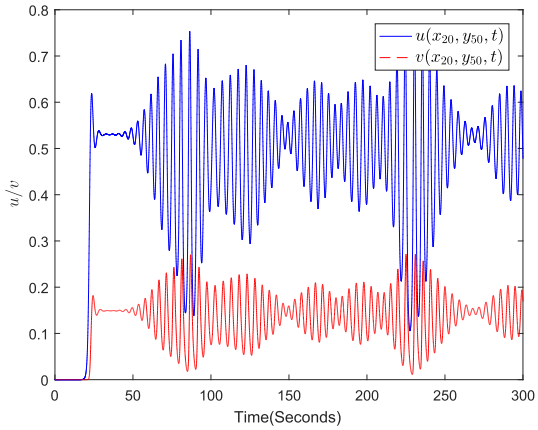

FIGURE 6. The trajectories of $u(x_{20}, y_{50}, t)$ and $v(x_{20}, y_{50}, t)$.

IV. SIMULATION RESULTS

To demonstrate the feasibility and effectiveness of the proposed method, simulation results on spiral waves with periodic and chaotic dynamics will be presented in the section.

The FHN model (6) will be first solved by using finite difference method and explicit Euler method. Eq. (7) is used to approximate the Laplacian $\nabla^2 u$. The reaction time terms

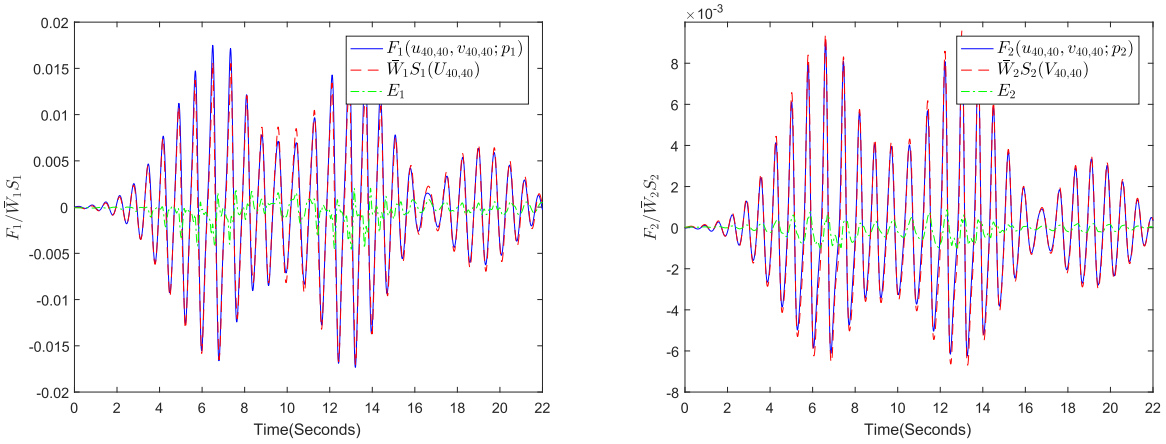

(a) The approximation of $F_1(u, v; p_1)$.

(b) The approximation of $F_2(u, v; p_2)$.

FIGURE 7. The identification results of $F_1(u, v; p_1)$ and $F_2(u, v; p_2)$ at the spatial point (x_{40}, y_{40}) corresponding to $h = 0.6$.

are stepped with the following algorithm:

$$\begin{cases} u^{k+1} = u^k + dt \cdot f(u^k, v^k) \\ v^{k+1} = v^k + dt \cdot g(u^k, v^k) \end{cases} \tag{18}$$

where $dt = t_{k+1} - t_k$ is the time step.

The FHN equation (6) is first solved under no-flux boundary conditions with the following parameters: $\Omega = [-30, 30] \times [-30, 30]$, $h = 0.6$, $N = 101$, $dt = 0.0001$, $\epsilon = 0.005, a = 0.3, b = 0.01, m = 1$. The numerical solution of the FHN model is a rotating wave which is rigidly rotating periodic states. The trajectory of $u(x, y, t)$ and $v(x, y, t)$ at spatial grid node (x_{26}, y_{26}) are shown in Figure 1, which are periodic.

The rectangle Ω is evenly subdivided into $(N-1)\times(N-1)$ subrectangles:

$$\Omega_{ij} = (x, y) : x_i \le x \le x_{i+1}, y_j \le y \le y_{j+1}$$

where

$$\begin{aligned} -L = x_1 < x_2 < \cdots \le x_N = L \\ -L = y_1 < y_2 < \cdots \le y_N = L \\ x_i = h \cdot (i - 51), \quad i = 1, \cdots, 101 \\ y_j = h \cdot (j - 51), \quad j = 1, \cdots, 101 \end{aligned}$$

Using the deterministic learning, $F_1(u_{i,j}, v_{i,j}; p)$ and $F_2(u_{i,j}, v_{i,j}; p)$ can be accurately identified and represented as $\bar{W}_1^T S_1(U_{i,j})$ and $\bar{W}_2^T S_2(V_{i,j})$. Figure 2 shows the identification results of $F_1(u, v; p_1)$ and $F_2(u, v; p_2)$ at the spatial grid point (x_{26}, y_{26}) by using deterministic learning as an example, where $E_1 = F_1(u_{26,26}, v_{26,26}; p_1) - \bar{W}_1^T S_1(U_{26,26})$ and $E_2 = F_2(u_{26,26}, v_{26,26}; p_1) - \bar{W}_2^T S_2(V_{26,26})$ are identification errors.

Based on the identification results at the spatial gird points (x_i, y_j), the system dynamics $F_1(u, v; p_1)$ and $F_2(u, v; p_2)$ corresponding to any spatial point (x, y) can be approximated by employing the proposed method. The interpolation approximation $\hat{F}_I(u, v; p_I)(I = 1, 2)$ at spatial points $(-15.3, -15.3)$ and $(23.7, -20.7)$ based on $\bar{W}_1^T S_1(U_{i,j})$ and $\bar{W}_2^T S_2(V_{i,j})(i, j = 1, \cdots, 101)$ are shown as examples in Figure 3 and Figure 4. It is shown that the accurate identification of $\widehat{F}_I(u, v); p_I)$ $(I = 1, 2)$ at any spatial point (x, y) can be achieved by employing the proposed method.

Another two numerical simulations with $h = 0.5$ and $h = 0.4$ are given to show the influence of h on the approximation error. Due to space limitation, the approximation results of $F_I(u, v; p_I)(I = 1, 2)$ at spatial points $(-15.3, -15.3)$ and $(23.7, -20.7)$ corresponding to $h = 0.5$ and $h = 0.4$ are omitted in the paper. $\|\widetilde{F}(u, v)\|_{L_1} = \|\widetilde{F}_1(u, v; p_1)\|_{L_1} + \|\widetilde{F}_2(u, v; p_2)\|_{L_1}$ is used to compare the approximation performance corresponding to different h, where $\|\cdot\|_{L_1}$ is the average L_1 norm, $\widetilde{F}_I(u, v; p_I) = \widehat{F}_I(u, v; p_I) - F_I(u, v; p_I), (I = 1, 2)$. $\|\widetilde{F}(u, v)\|_{L_1}$ at spatial points $(-15.3, -15.3)$ and $(23.7, -20.7)$ corresponding to $h = 0.4$, $h = 0.5$, and $h = 0.6$ are given in Figure 5. It can be seen that the smaller mesh spacing h, the smaller the approximation error $\epsilon_{N1}(x)$, $\epsilon_{N2}(x)$. In other words, the smaller h, the higher accuracy of approximation of the proposed method.

For spiral waves with chaotic orbit, the accurately identification of FHN model can also be achieved. Spiral waves with chaotic behavior can be generated from FHN model (6) under the following parameter conditions: $\epsilon = 0.2$, $h = 0.6$, $N = 101$, $dt = 0.01$, $a = 0.3$, $b = 0.01$, $m = 3$. The chaotic orbit of spiral waves at spatial grid node (x_{20}, y_{50}) is shown in Fig. (III-B) as an example. The identification results of $F_1(u, v; p_1)$ and $F_2(u, v; p_2)$ at spatial grid node (x_{40}, y_{40}) by using deterministic learning are shown in Figure 7, where $E_1 = F_1(u_{40,40}, v_{40,40}; p_1) - \bar{W}_1^T S_1(U_{40,40})$ and $E_2 = F_2(u_{40,40}, v_{40,40}; p_1) - \bar{W}_2^T S_2(V_{40,40})$ are identification errors.

The accurate approximation of $F_1(u, v; p_1)$ and $F_2(u, v; p_2)$ at spatial points $(11.7, 11.7)$ and $(23.7, 23.4)$ using

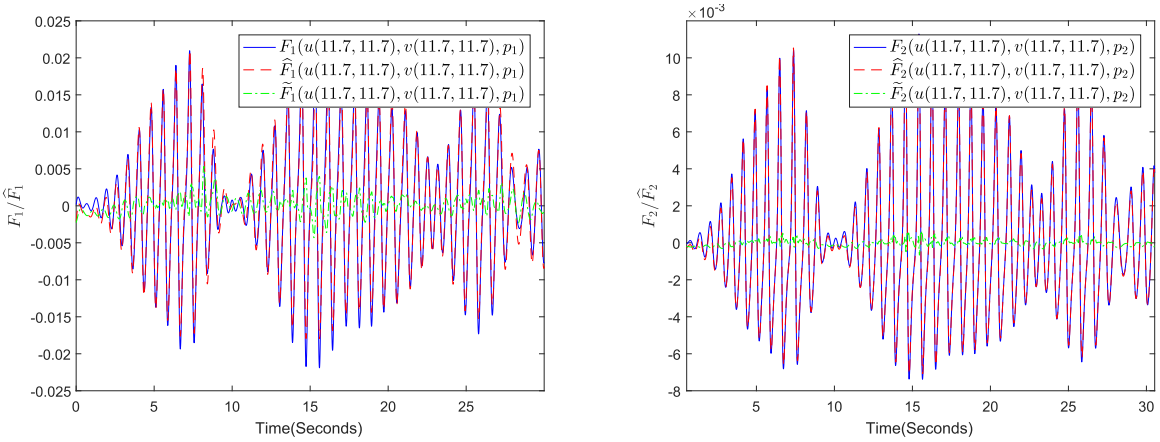

FIGURE 8. The approximation of $F_1(u, v; p_1)$ and $F_2(u, v; p_2)$ with chaotic $u(x, y, t)$ and $v(x, y, t)$ at spatial point (11.7, 11.7).

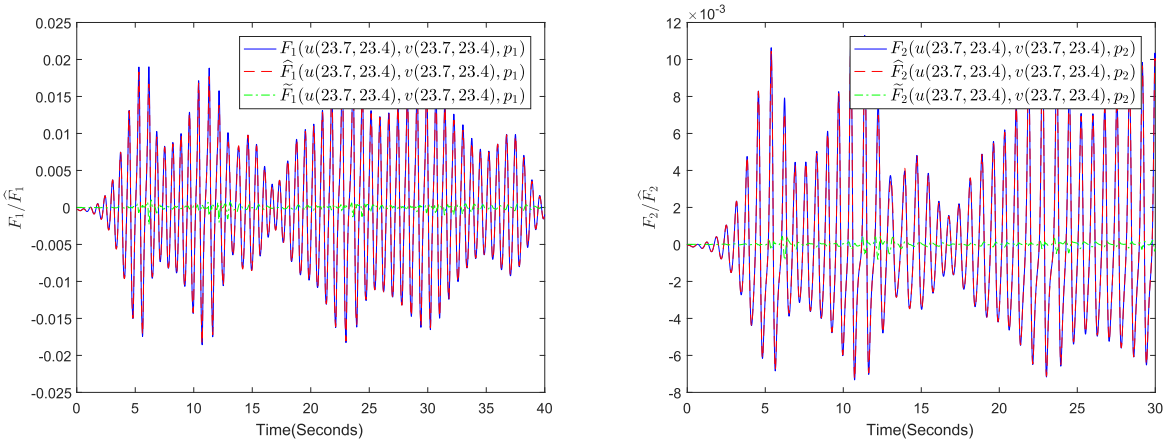

(a) The approximation of $F_1(u, v; p_1)$ (b) The approximation of $F_2(u, v; p_1)$

FIGURE 9. The approximation of $F_1(u, v; p_1)$ and $F_2(u, v; p_2)$ with chaotic $u(x, y, t)$ and $v(x, y, t)$ at spatial point (23.7, 23.4).

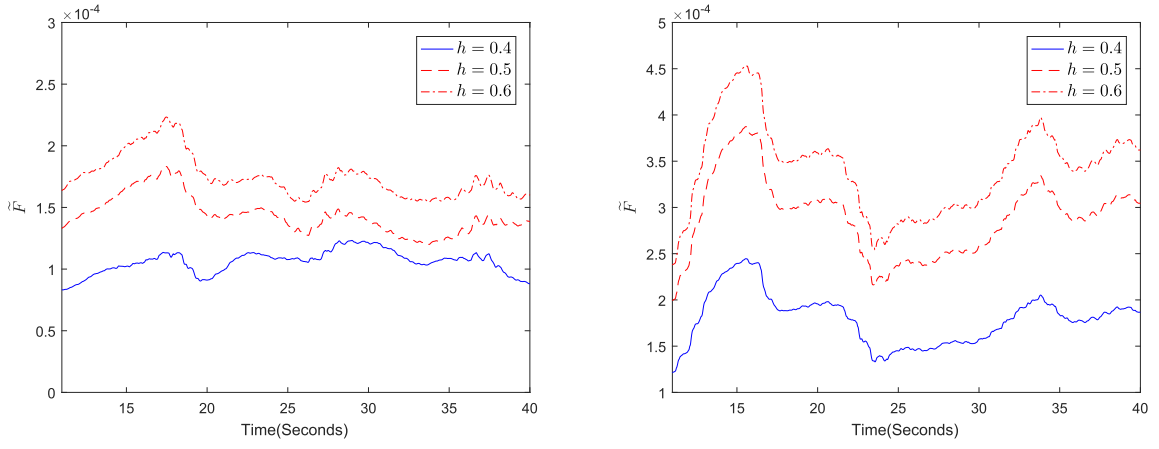

(a) (b)

FIGURE 10. The approximation performance comparison of different h. a: $\|\widetilde{F}(u(11.7, 11.7), v(11.7, 11.7))\|_{L_1}$ corresponding to different h; b: $\|\widetilde{F}(u(23.7, 23.4), v(23.7, 23.4))\|_{L_1}$ corresponding to different h.

bicubic spline interpolation based on $\bar{W}_1^T S_1(U_{i,j})$ and $\bar{W}_2^T S_2(V_{i,j})(i, j = 1, \cdots, 101)$ are shown in shown as examples in Figures 8, and 9 corresponding to $h = 0.6$, respectively. These indicate that $F_I(u, v; p_I)(I = 1, 2)$ with chaotic orbit of $u(x, y, t)$ and $v(x, y, t)$ can also be accurately identified by using the proposed method. The comparisons

of $\|\widetilde{F}(u,v)\|_{L_1}$ at spatial points (11.7, 11.7) and (23.7, 23.4) corresponding to $h = 0.4, 0.5, 0.6$ are shown in Figure 10. It can be seen the smaller mesh spacing h, the smaller approximation error, which is consistent with the influence of h on approximation error for periodic orbit.

V. CONCLUSION

In this study, a novel method via deterministic learning and interpolation is proposed for identifying FHN model dynamics. It extends the method proposed in [29] from one-dimensional DPS to a two-dimensional DPS with coupled variables, and achieves the global identification of the FHN model based on system states at a set of spatial points. It also provides a new idea for the identification of other actual DPS. It is a significant advancement from the viewpoint of the possible application of the method in the identification of actual DPS (e.g., the studies of spiral wave in cardiac tissue). The system dynamics at spatial grid nodes are first accurately modeled by employing deterministic learning. Then the system dynamics at any other spatial point is approximated based on the identification results corresponding to the spatial grid nodes. That is, global identification of the FHN model dynamics is achieved. The effectiveness and feasibility of the proposed method are demonstrated theoretically and numerically, which involves reselecting the interpolation method and correspondingly both theoretical derivation and computer algorithm have to be redesigned due to the FHN model is composed of two coupled PDEs. Different from existing methods in literature, the identification results contain more information than system structure and parameters of the FHN model. In addition, the identification result can be represented and stored as a constant manner, which makes it easy to be employed to recognize the similar dynamical behaviors. The proposed method can also provide some new thought in practical application, such as study of spiral wave in cardiac tissue. Future work will be focused on the following two aspects: (a) how to extend the method to other high-dimensional DPS; (b) how to improve the approximation performance through the appropriate selection of dimensionality reduction method and interpolation algorithm.

APPENDIX A

In the appendix, we give the proof of Theorem 7.

Proof: From (14), it can be seen that $\frac{\partial^{k+l}W_1(x,y,t)}{\partial x^k\partial y^l}$ $\left(\frac{\partial^{k+l}W_2(x,y,t)}{\partial x^k\partial y^l}\right)$ is bounded and continuous if and only if $\frac{\partial^{k+l}\tilde{u}(x,y,t)}{\partial x^k\partial y^l}$ $\left(\frac{\partial^{k+l}\tilde{v}(x,y,t)}{\partial x^k\partial y^l}\right)$ and $\frac{\partial^{k+l}S_1(U(x,y,t))}{\partial x^k\partial y^l}$ $\left(\frac{\partial^{k+l}S_2(V(x,y,t))}{\partial x^k\partial y^l}\right)$ are bounded and continuous.

i) We first prove that $\frac{\partial^{k+l}\tilde{u}(x,y,t)}{\partial x^k\partial y^l}$ is bounded in space domain Ω.

Assume $\frac{\partial\tilde{u}(x,y,t)}{\partial x}$ is unbounded in Ω, then for $\forall \mathbf{M}_{1,0} > 0$, without loss of generality, $\exists(x', y') = (x_i, y_j) \in \Omega$, such that

$$\left|\frac{\partial\tilde{u}(x_i,y_j,t)}{\partial x}\right| = \left|\lim_{\triangle x\to 0}\frac{\tilde{u}(x_{i+1},y_j,t)-\tilde{u}(x_i,y_j,t)}{\triangle x}\right| > \mathbf{M}_{1,0} \tag{19}$$

then we have

$$|\tilde{u}(x_{i+1},y_j,t)-\tilde{u}(x_i,y_j,t)| > \triangle x\mathbf{M}_{1,0} \tag{20}$$

According to Theorem 4, for $(x_i, y_j) \in \Omega$

$$\lim_{t\to\infty}\tilde{u}(x_i,y_j,t) = 0$$

thus

$$\lim_{t\to\infty}\|\tilde{u}(x_{i+1},y_j,t)-\tilde{u}(x_i,y_j,t)\| \le \lim_{t\to\infty}\|\tilde{u}(x_{i+1},y_j,t)\| + \lim_{t\to\infty}\|\tilde{u}(x_i,y_j,t)\| \le 0$$

It contradicts with (20). Thus, $\frac{\partial\tilde{u}(x,y,t)}{\partial x}$ is bounded in Ω

Assume that $\frac{\partial^2\tilde{u}(x,y,t)}{\partial x^2}$ is unbounded in Ω, then for $\forall \mathbf{M}_{2,0} > 0$, without loss of generality, there $\exists(x', y') = (x_i, y_j) \in \Omega$, such that

$$\begin{aligned}\left|\frac{\partial^2\tilde{u}(x_i,y_j,t)}{\partial x^2}\right| &= \left|\lim_{\triangle x\to 0}\frac{\frac{\partial\tilde{u}(x_{i+1},y_j,t)}{\partial x}-\frac{\partial\tilde{u}(x_i,y_j,t)}{\partial x}}{\triangle x}\right| \\ &= \left|\lim_{\triangle x\to 0}\frac{\tilde{u}(x_{i+2},y_j,t)-2\tilde{u}(x_{i+1},y_j,t)+\tilde{u}(x_i,y_j,t)}{\triangle x^2}\right|\end{aligned} \tag{21}$$

then we have

$$|\tilde{u}(x_{i+2},y_j,t)-2\tilde{u}(x_{i+1},y_j,t)+\tilde{u}(x_i,y_j,t)| > \triangle x^2\mathbf{M}_{2,0}$$

Similarly, It contradicts with Theorem 4 that $\tilde{u}_{i,j}$ converges to a small neighborhood of zero. Hence, $\frac{\partial^2\tilde{u}(x,y,t)}{\partial x^2}$ is bounded.

In the same way, we can prove that $\frac{\partial^k\tilde{u}(x,y,t)}{\partial x^k}(k = 3, 4)$ and $\frac{\partial^l\tilde{u}(x,y,t)}{\partial y^l}(l = 1, 2, 3, 4)$ are all bounded in Ω.

Assume that $\frac{\partial^{1+l}\tilde{u}(x,y,t)}{\partial x\partial y^l}$ is unbounded in Ω, then for $\forall \mathbf{M}_{1,l} > 0$, without loss of generality, there $\exists(x', y') \in \Omega$, such that

$$\left|\frac{\partial^{1+l}\tilde{u}(x',y',t)}{\partial x\partial y^l}\right| = \left|\lim_{\triangle x\to 0}\frac{\frac{\partial^l\tilde{u}(x'+\triangle x,y',t)}{\partial y^l}-\frac{\partial^l\tilde{u}(x',y',t)}{\partial y^l}}{\triangle x}\right| > \mathbf{M}_{1,l} \tag{22}$$

It contradicts with the boundness of $\frac{\partial^l\tilde{u}(x,y,t)}{\partial y^l}$ proved above.

Assume that $\frac{\partial^{2+l}\tilde{u}(x,y,t)}{\partial x^2\partial y^l}$ is unbounded in Ω, without loss of generality, there $\exists(x', y') \in \Omega$, such that

$$\left|\frac{\partial^{2+l}\tilde{u}(x',y',t)}{\partial x^2\partial y^l}\right| = \left|\lim_{\triangle x\to 0}\frac{\frac{\partial^{1+l}\tilde{u}(x'+\triangle x,y',t)}{\partial x\partial y^l}-\frac{\partial^{1+l}\tilde{u}(x',y',t)}{\partial x\partial y^l}}{\triangle x}\right| > \mathbf{M}_{2,l} \tag{23}$$

It contradicts with the boundness of $\frac{\partial^{1+l}\tilde{u}(x,y,t)}{\partial x\partial y^l}$ proofed above. Similarly, the boundness of $\frac{\partial^{l+k}\tilde{u}(x,y,t)}{\partial x^k\partial y^l}(k = 3, 4)$ can also be proofed.

In summary, $\frac{\partial^{k+l}\tilde{u}(x,y,t)}{\partial x^k \partial y^l}$ is bounded in Ω, that is there exists $\widetilde{M}_u^{k,l} > 0$, so that for $\forall (x, y) \in \Omega$,

$$\frac{\partial^{k+l}\tilde{u}(x, y, t)}{\partial x^k \partial y^l} < \widetilde{M}_u^{k,l}, \quad 0 \le k, l \le 4$$

In the same way, it can be proofed that $\frac{\partial^{k+l}\tilde{v}(x,y,t)}{\partial x^k \partial y^l}$, $0 \le k, l \le 4$ is bounded in Ω, that is there exists $\widetilde{M}_v^{k,l} > 0$, so that for $\forall (x, y) \in \Omega$,

$$\frac{\partial^{k+l}\tilde{v}(x, y, t)}{\partial x^k \partial y^l} < \widetilde{M}_v^{k,l}, \quad 0 \le k, l \le 4$$

ii) Next, we prove the continuity of $\frac{\partial^{k+l}\tilde{u}(x,y,t)}{\partial x^k \partial y^l}$.

From the above analysis, it can be proved that $\frac{\partial^{k+l+2}\tilde{u}(x,y,t)}{\partial x^{k+1} \partial y^{l+1}}$ is also bounded in Ω, that is there exists $\widetilde{M}_u^{k+1,l+1} > 0$ such that

$$\left|\frac{\partial^{k+l+2}\tilde{u}(x, y, t)}{\partial x^{k+1} \partial y^{l+1}}\right| \le \widetilde{M}_u^{k+1,l+1}$$

For $\forall \epsilon > 0$, no matter how small, take $\delta = (\frac{\epsilon}{\widetilde{M}_u^{k+1,l+1}})^{\frac{1}{2}} > 0$, for $(x', y'), (x'', y'') \in \Omega$, if $|x' - x''| < \delta$ and $|y' - y''| < \delta$, we have

$$\begin{aligned}
&\left|\frac{\partial^{k+l}\tilde{u}(x'', y'', t)}{\partial x^k \partial y^l} - \frac{\partial^{k+l}\tilde{u}(x', y', t)}{\partial x^k \partial y^l}\right| \\
&= \left|\int_{y'}^{y''}\int_{x'}^{x''} \frac{\partial^{k+l+2}\tilde{u}(x, y, t)}{\partial x^{k+1} \partial y^{l+1}} dxdy\right| \\
&\le \widetilde{M}_u^{k+1,l+1} \cdot |x'' - x'| \cdot |y'' - y'| \\
&< \widetilde{M}_u^{k+1,l+1} \cdot \delta^2 = \epsilon
\end{aligned} \tag{24}$$

That is, $\frac{\partial^{k+l}\tilde{u}(x,y,t)}{\partial x^k \partial y^l}$ is continus in Ω.

Similarity, the continuity of $\frac{\partial^{k+l}\tilde{v}(x,y,t)}{\partial x^k \partial y^l}$ can also be proofed.

iii) The continuity of $\frac{\partial^{k+l}S_1(U(x,y,t))}{\partial x^k \partial y^l}$ is apparent, since $u(x, y, t), v(x, y, t) \in C^{4,4}(\Omega) \times [0, \infty)$ and $S_1(U(x, y, t))$ is a vector of Gaussian function. As $\Omega = [-L, L] \times [-L, L]$ is a closed region, $\frac{\partial^{k+l}S(U(x,y,t))}{\partial x^k \partial y^l}$ is bounded in Ω. There exists a constant $\mathbf{S}_1^{k,l} > 0$, such that, for $\forall (x, y) \in \Omega$

$$\left\|\frac{\partial^{k+l}S_1(U(x, y, t))}{\partial x^k \partial y^l}\right\|_\infty \le \mathbf{S}_1^{k,l}. \tag{25}$$

In the same way, there exists a constant $\mathbf{S}_2^{k,l} > 0$, such that, for $\forall (x, y) \in \Omega$,

$$\left\|\frac{\partial^{k+l}S_2(V(x, y, t))}{\partial x^k \partial y^l}\right\|_\infty \le \mathbf{S}_2^{k,l}. \tag{26}$$

iv) With continuity of $\frac{\partial^{k+l}\tilde{u}(x,y,t)}{\partial x^k \partial x^l}$ and $\frac{\partial^{k+l}S_1(U(x,y,t))}{\partial x^k \partial y^l}$, it can be derived that $\frac{\partial^{k+l}\hat{W}_1(x,y,t)}{\partial x^k \partial y^l}$ is continuous and bounded in Ω, that is $W_1(x, y, t) \in C^{(4,4)}(\Omega) \times [0, \infty]$, and there exists a constant $\mathbf{W}_1^{k,l} > 0$, such that for $\forall (x, y) \in \Omega$,

$$\left\|\frac{\partial^{k+l}W_1(x, y, t)}{\partial x^k \partial y^l}\right\|_\infty \le \mathbf{W}_1^{k,l}. \tag{27}$$

Similarity, $\frac{\partial^{k+l}W_2(x,y,t)}{\partial x^k \partial y^l}$ is also continuous and bounded in Ω, there exists a constant $\mathbf{W}_2^{k,l} > 0$, such that for $\forall (x, y) \in \Omega$,

$$\left\|\frac{\partial^{k+l}W_2(x, y, t)}{\partial x^k \partial y^l}\right\|_\infty \le \mathbf{W}_2^{k,l}. \tag{28}$$

■

APPENDIX B

In the appendix, we give the proof of Theorem 8.

Proof: By Theorem 4, it can be seen that the dynamics $F_1(u, v; p)$ can be accurately modeled by using deterministic learning and expressed as follow:

$$F_1(u, v; p_1) = W_1(x, y, T)S_1(U, T) + \epsilon_I(x, y) \tag{29}$$

where T is a time point to confirm $W_1(x, y, t)$ convergence, $\epsilon_I(x, y) = O(\epsilon_I)$ is the approximation error.

By Theorem 7 and Lemma 6

$$\begin{cases} W_1(x, y, T) = W_{1_C}(x, y, T) + R_{1_W}(x, y, T) \\ S_1(U(x, y, T)) = S_{1_C}(x, y, T) + R_{1_S}(x, y, T) \end{cases} \tag{30}$$

and

$$\begin{cases} \|R_{1_W}(x, y, T)\|_\infty \le \frac{5h_x^4}{384}\|W_1^{(4,0)}\|_\infty + \frac{81h_x^2h_y^2}{64}\|W_1^{(2,2)}\|_\infty \\ + \frac{5h_y^4}{384}\|W_1^{(0,4)}\|_\infty \\ \|R_{1_S}(x, y, T)\|_\infty \le \frac{5h_x^4}{384}\|S_1^{(4,0)}\|_\infty + \frac{81h_x^2h_y^2}{64}\|S_1^{(2,2)}\|_\infty \\ + \frac{5h_y^4}{384}\|S_1^{(0,4)}\|_\infty \end{cases} \tag{31}$$

Thus

$$\begin{aligned}
F_1(u, v; p_1) &= W_1(x, y, t)S_1(U(x, y, T)) + \epsilon(x, y) \\
&= (W_{1_C}(x, y, T) + R_{1_W}(x, y, T))(S_{1_C}(x, y, T) \\
&\quad + R_{1_S}(x, y, T)) + O(\epsilon_I) \\
&= W_{1_C}(x, y, T)S_{1_C}(x, y, T) + \epsilon_{N_1}(x, y)
\end{aligned} \tag{32}$$

where

$$\begin{aligned}
\epsilon_{N_1}(x) = W_{1_C}(x, y, T)R_{1_S}(x, y, T) \\
+R_{1_W}(x, y, T)S_1(U(x, y, T)) + O(\epsilon_I)
\end{aligned}$$

.

According to Theorem 7 and Lemma 6

$$\begin{aligned}
&\|R_{1_W}(x, y, T)S_1(U(x, y, T))\|_\infty \\
&\le \|R_{1_W}(x, y, T)\|_\infty \|S_1(U(x, y, T))\|_\infty \\
&\le \|R_{1_W}(x, y, T)\|_\infty \\
&\le \frac{5h_x^4}{384}\mathbf{W}_1^{4,0} + \frac{81h_x^2h_y^2}{64}\mathbf{W}_1^{2,2} + \frac{5h_y^4}{384}\mathbf{W}_1^{0,4}
\end{aligned} \tag{33}$$

and

$$\begin{aligned}
&\|W_{1_C}(x, y, T)R_{1_S}(x, y, T)\|_\infty \\
&\le \|W_{1_C}(x, y, T)\|_\infty (\frac{5h_x^4}{384}\mathbf{S}_1^{4,0} + \frac{81h_x^2h_y^2}{64}\mathbf{S}_1^{2,2} + \frac{5h_y^4}{384}\mathbf{S}_1^{0,4})
\end{aligned} \tag{34}$$

Thus,

$$\begin{aligned}&\|\epsilon_{N_1}(x)\|_\infty\\&\quad\le\frac{5h_x^4}{384}(\mathbf{W}_1^{4,0}+\mathbf{S}_1^{4,0}\|W_{1_C}(x,y,T)\|_\infty)\\&\qquad+\frac{81h_x^2h_y^2}{64}(\mathbf{W}_1^{2,2}+\mathbf{S}_1^{2,2}\|W_{1_C}(x,y,T)\|_\infty\\&\qquad+\frac{5h_y^4}{384}(\mathbf{W}_1^{0,4}+\mathbf{S}_1^{0,4}\|W_{1_C}(x,y,T)\|_\infty)+O(\epsilon_I)\end{aligned}\tag{35}$$

By (14), (30) and (31),

$$\begin{aligned}&\|W_{1_C}(x,y,T)\|_\infty\\&\quad=\|W_1(x,y,T)-R_{1_W}(x,y,T)\|_\infty\\&\quad\le\|W_1(x,y,T)\|_\infty+\|R_{1_W}(x,y,T)\|\\&\quad\le(C_1+T\|\Gamma_1\|_\infty\|\tilde{u}(x,y,T)\|_\infty)+\frac{5h_x^4}{384}\mathbf{W}_1^{4,0}\\&\qquad+\frac{81h_x^2h_y^2}{64}\mathbf{W}_1^{2,2}+\frac{5h_y^4}{384}\mathbf{W}_1^{0,4}\end{aligned}\tag{36}$$

thus, $\|W_{1_C}(x,y,T)\|_\infty$ is boundness in Ω

By the boundness of $\mathbf{W}_1^{4,0}$, $\mathbf{W}_1^{2,2}$, $\mathbf{W}_1^{0,4}$, $\mathbf{S}_1^{4,0}$, $\mathbf{S}_1^{2,2}$, $\mathbf{S}_1^{0,4}$ and $\|W_{1_C}(x,y,T)\|_\infty$, we have $W_{1_C}(x,y,T)S_{1_C}(x,y,T)$ converges uniformly to $W_1(x,y,T)S_1(U(x,y,T))$ as $h=\max\{h_x,h_y\}\to 0$, and

$$\lim_{h\to 0}\|\epsilon_{N_1}(x,y)\|_\infty=O(\epsilon_1).\tag{37}$$

Similarly, it can be proved that $W_{2_C}(x,y,T)S_{2_C}(x,y,T)$ converges uniformly to $W_2(x,y,T)S_2(V(x,y,T))$ as $h=\max\{h_x,h_y\}\to 0$, and

$$\lim_{h\to 0}\|\epsilon_{N_2}(x,y)\|_\infty=O(\epsilon_2).\tag{38}$$

■

REFERENCES

[1] F. H. Fenton, E. M. Cherry, H. M. Hastings, and S. J. Evans, "Multiple mechanisms of spiral wave breakup in a model of cardiac electrical activity," *Chaos, Interdiscipl. J. Nonlinear Sci.*, vol. 12, no. 3, pp. 852–892, 2002.

[2] M. Bär, "Reaction-diffusion patterns and waves: From chemical reactions to cardiac arrhythmias," in *Spirals Vortices*. Cham, Switzerland: Springer, 2019, pp. 239–251.

[3] M. O. Gani and T. Ogawa, "Spiral breakup in a RD system of cardiac excitation due to front–back interaction," *Wave Motion*, vol. 79, pp. 73–83, Jun. 2018.

[4] R. FitzHugh, "Impulses and physiological states in theoretical models of nerve membrane," *Biophys. J.*, vol. 1, no. 6, pp. 445–466, 1961.

[5] J. Nagumo, S. Arimoto, and S. Yoshizawa, "An active pulse transmission line simulating nerve axon," *Proc. IRE*, vol. 50, no. 10, pp. 2061–2070, Oct. 1962.

[6] A. L. Hodgkin and A. F. Huxley, "A quantitative description of membrane current and its application to conduction and excitation in nerve," *J. Physiol.*, vol. 117, no. 4, pp. 500–544, 1952.

[7] S. Guo, Q. Dai, H. Cheng, H. Li, F. Xie, and J. Yang, "Spiral wave chimera in two-dimensional nonlocally coupled Fitzhugh–Nagumo systems," *Chaos, Solitons Fractals*, vol. 114, pp. 394–399, Sep. 2018.

[8] L. Lü, L. Ge, L. Gao, C. Han, and C. Li, "Synchronization transmission of spiral wave and turbulence in uncertain time-delay neuronal networks," *Phys. A, Stat. Mech. Appl.*, vol. 525, pp. 64–71, Jul. 2019.

[9] H. Liang and H. Wu, "Parameter estimation for differential equation models using a framework of measurement error in regression models," *J. Amer. Stat. Assoc.*, vol. 103, no. 484, pp. 1570–1583, 2008.

[10] A. Concha and R. Garrido, "Parameter estimation of the Fitzhugh–Nagumo neuron model using integrals over finite time periods," *J. Comput. Nonlinear Dyn.*, vol. 10, no. 2, 2015, Art. no. 021023.

[11] H.-X. Li and C. Qi, "Modeling of distributed parameter systems for applications—A synthesized review from time–space separation," *J. Process Control*, vol. 20, no. 8, pp. 891–901, 2010.

[12] D. Coca and S. A. Billings, "Direct parameter identification of distributed parameter systems," *Int. J. Syst. Sci.*, vol. 31, no. 3, pp. 11–17, 2000.

[13] H. T. Banks and K. Kunisch, *Estimation Techniques for Distributed Parameter Systems*. Berlin, Germany: Springer, 2012.

[14] E. Blanchard, A. Sandu, and C. Sandu, "Parameter estimation for mechanical systems via an explicit representation of uncertainty," *Eng. Comput.*, vol. 26, no. 5, pp. 541–569, 2009.

[15] E. Blanchard, A. Sandu, and C. Sandu, "A polynomial chaos-based Kalman filter approach for parameter estimation of mechanical systems," *J. Dyn. Syst., Meas., Control*, vol. 132, no. 6, 2010, Art. no. 061404.

[16] A. Sandu, C. Sandu, and M. Ahmadian, "Modeling multibody systems with uncertainties. Part I: Theoretical and computational aspects," *Multibody Syst. Dyn.*, vol. 15, no. 4, pp. 369–391, 2006.

[17] A. Ghosh, V. R. Kumar, and B. D. Kulkarni, "Parameter estimation in spatially extended systems: The Karhunen-Lóeve and Galerkin multiple shooting approach," *Phys. Rev. E, Stat. Phys. Plasmas Fluids Relat. Interdiscip. Top.*, vol. 64, no. 5, 2001, Art. no. 056222.

[18] H. M. Park, T. H. Kim, and D. H. Cho, "Estimation of parameters in flow reactors using the Karhunen–Loève decomposition," *Comput. Chem. Eng.*, vol. 23, no. 1, pp. 109–123, 1998.

[19] J. A. Pitt and J. R. Banga, "Parameter estimation in models of biological oscillators: An automated regularised estimation approach," *BMC Bioinf.*, vol. 20, no. 1, p. 82, 2019.

[20] Y. Zhao, S. A. Billings, D. Coca, Y. Guo, R. Ristic, and L. Dematos, "Identification of a temperature dependent FitzHugh–Nagumo model for the Belousov–Zhabotinskii reaction," *Int. J. Bifurcation Chaos*, vol. 21, no. 11, pp. 3249–3258, 2011.

[21] Y. He and D. E. Keyes, "Reconstructing parameters of the FitzHugh–Nagumo system from boundary potential measurements," *J. Comput. Neurosci.*, vol. 23, no. 2, pp. 251–264, 2007.

[22] S. Berg, S. Luther, and U. Parlitz, "Synchronization based system identification of an extended excitable system," *Chaos, Interdiscipl. J. Nonlinear Sci.*, vol. 21, no. 3, 2011, Art. no. 033104.

[23] C. Wang, T.-R. Chen, and T.-F. Liu, "Deterministic learning and data-based modeling and control," *Acta Autom. Sinica*, vol. 35, no. 6, pp. 693–706, 2009.

[24] L. P. Shil'nikov, *Methods of Qualitative Theory in Nonlinear Dynamics Part I*, vol. 5. Singapore: World Scientific, 2001.

[25] C. Wang and D. J. Hill, "Learning from neural control," *IEEE Trans. Neural Netw.*, vol. 17, no. 1, pp. 130–146, Jan. 2006.

[26] C. Wang and D. J. Hill, "Deterministic learning and rapid dynamical pattern recognition," *IEEE Trans. Neural Netw.*, vol. 18, no. 3, pp. 617–630, May 2007.

[27] C. Wang and D. J. Hill, *Deterministic Learning Theory for Identification, Recognition, and Control*. Boca Raton, FL, USA: CRC Press, 2009.

[28] X. Dong and C. Wang, "Identification of the FitzHugh–Nagumo model dynamics via deterministic learning," *Int. J. Bifurcation Chaos*, vol. 25, no. 12, p. 1550159, 2015.

[29] X. Dong, C. Wang, Q. Yang, and W. Si, "System identification of distributed parameter system with recurrent trajectory via deterministic learning and interpolation," *Nonlinear Dyn.*, vol. 95, no. 1, pp. 73–86, 2019.

[30] A. Ralston and P. Rabinowitz, *A First Course in Numerical Analysis*. North Chelmsford, MA, USA: Courier Corporation, 2001.

[31] R. L. Burden and J. D. Faires, *Numerical Analysis*. Seattle, WA, USA: Brooks, 2001.

[32] D.-J. Kang, F. Chen, and J.-H. Park, "New measurement method of Poisson's ratio of thin films by applying digital image correlation technique," *Int. J. Precis. Eng. Manuf.*, vol. 15, no. 5, pp. 883–888, 2014.

[33] N. S.-N. Lam, "Spatial interpolation methods: A review," *Amer. Cartographer*, vol. 10, no. 2, pp. 129–150, 1983.

[34] C. Caruso and F. Quarta, "Interpolation methods comparison," *Comput. Math. Appl.*, vol. 35, no. 12, pp. 109–126, 1998.

[35] I. V. Biktasheva, A. V. Holden, and V. N. Biktashev, "Localization of response functions of spiral waves in the FitzHugh–Nagumo system," *Int. J. Bifurcation Chaos Appl. Sci. Eng.*, vol. 16, no. 5, pp. 1547–1555, 2006.

[36] Y. A. Kuznetsov, *Elements of Applied Bifurcation Theory*. New York, NY, USA: Springer-Verlag, 1998.
[37] R. E. Carlson and C. A. Hall, "Error bounds for bicubic spline interpolation," *J. Approximation Theory*, vol. 7, no. 1, pp. 41–47, 1973.

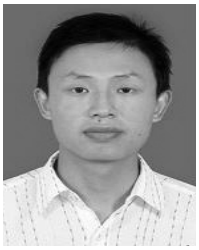

XUNDE DONG received the M.Sc. degree in mathematical and applied mathematical and the Ph.D. degree in control theory and control engineering from the South China University of Technology, Guangzhou, China, in 2010 and 2014, respectively, where he is currently an Assistant Professor with the School of Automation Science and Engineering. His research interests include distributed parameter systems, nonlinear adaptive control, and dynamical pattern recognition.

WENJIE SI received the B.Sc. and M.Sc. degrees in control theory and control engineering from Zhengzhou University, Zhengzhou, China, in 2008 and 2011, respectively, and the Ph.D. degree in control theory and control engineering from the South China University of Technology, Guangzhou, China, in 2015. He is currently an Assistant Professor with the School of Electrical and Control Engineering, Henan University of Urban Construction. His current research interests include adaptive neural control, nonlinear adaptive control, and deterministic learning theory.

CONG WANG received the B.E. and M.E. degrees from the Beijing University of Aeronautics and Astronautics, in 1989 and 1997, respectively, and the Ph.D. degree from the Department of Electrical and Computer Engineering, National University of Singapore, in 2002. From 2001 to 2004, he did his Postdoctoral Research with the Department of Electronic Engineering, City University of Hong Kong. He is currently a Professor with the School of Automation Science and Engineering, South China University of Technology, Guangzhou, China. His research interests include intelligent control, neural networks, nonlinear systems and control, dynamical pattern recognition, pattern-based control, dynamical systems, and oscillation fault diagnosis.